University of Reading

A brain-wave equation incorporating axo-dendritic connectivity

Article

Accepted Version

Ross, J., Margetts, M., Bojak, I. ORCID: https://orcid.org/0000-0003-1765-3502, Nicks, R., Avitabile, D. and Coombes, S. (2020) A brain-wave equation incorporating axo-dendritic connectivity. Physical Review E, 101 (2). 022411. ISSN 2470-0045 doi: 10.1103/PhysRevE.101.022411 Available at https://centaur.reading.ac.uk/88781/

It is advisable to refer to the publisher's version if you intend to cite from the work. See Guidance on citing.
Published version at: https://journals.aps.org/pre/abstract/10.1103/PhysRevE.101.022411
To link to this article DOI: http://dx.doi.org/10.1103/PhysRevE.101.022411

Publisher: American Physical Society

All outputs in CentAUR are protected by Intellectual Property Rights law, including copyright law. Copyright and IPR is retained by the creators or other copyright holders. Terms and conditions for use of this material are defined in the End User Agreement.

www.reading.ac.uk/centaur

CentAUR

University of Reading

Central Archive at the University of Reading

Reading's research outputs online

A brain-wave equation incorporating axo-dendritic connectivity

James Ross,[1,*] Michelle Margetts,[1,†] Ingo Bojak,[2,‡] Rachel Nicks,[1,§] Daniele Avitabile,[3,4,¶] and Stephen Coombes[1,**]

[1] *Centre for Mathematical Medicine and Biology, School of Mathematical Sciences, University of Nottingham, NG7 2RD, UK.*
[2] *School of Psychology & Clinical Language Sciences, University of Reading, Reading RG6 6AL, UK.*
[3] *Department of Mathematics, Vrije Universiteit (VU University Amsterdam), Faculteit der Exacte Wetenschappen, De Boelelaan 1081a, 1081 HV Amsterdam, The Netherlands.*
[4] *Mathneuro Team, Inria Sophia Antipolis, 2004 Rue des Lucioles, 06902 Sophia Antipolis, Cedex, France.*

(Dated: January 20, 2020)

We introduce an integral model of a two-dimensional neural field that includes a third dimension representing space along a dendritic tree that can incorporate realistic patterns of axo-dendritic connectivity. For natural choices of this connectivity we show how to construct an equivalent brain-wave partial differential equation that allows for efficient numerical simulation of the model. This is used to highlight the effects that passive dendritic properties can have on the speed and shape of large scale traveling cortical waves.

Keywords: Neural field, EEG modelling, Brain wave equation, dendritic cable

I. INTRODUCTION

Ever since Hans Berger made the first recording of the human electroencephalogram (EEG) in 1924 there has been a tremendous interest in understanding the physiological basis of brain rhythms [1]. This has included the development of so-called neural field models, recently reviewed in [2], for the forward generation of EEG signals as well as the use of techniques from spatio-temporal pattern formation [3], and nonequilibrium phase transitions [4] for their analysis. These neural field models are often formulated in terms of delayed integro-differential equations posed on appropriate surfaces, including lines [5], planes [6], and folded cortical structures [7].

At heart modern biophysical theories assert that EEG signals from a single scalp electrode arise from the coordinated activity of $\sim 10^8$ pyramidal cells in cortex [8]. These are arranged with their dendrites roughly in parallel and perpendicular to the cortical surface. Synaptic activation at the dendrites creates a net ionic membrane current representing a sink (source) for excitatory (inhibitory) synapses with a negative (positive) extracellular potential. Because there is no long-term accumulation of charge in the tissue, this synaptic current flowing inside the cell escapes across the membrane again as a return current, in particular in places with large surface area like the soma. This creates a distributed extracellular source in the case of a synaptic sink and vice-versa for a synapse that acts as a source. Due to the elongated morphology of pyramidal neurons, the separation of sink and source typically leads to the effective formation of a current dipole. Hence, at the population level the potential field generated by a synchronously activated population of cortical pyramidal cells behaves like that of a current dipole layer. Although the important contribution that single dendritic trees make to generating extracellular electric field potentials has been realized for some time, and can be calculated using Maxwell's equations [9], they are typically not accounted for in neural field models. For example in the Nunez model [10] for the generation of the α-rhythm neuronal cell types are arranged in sheets, with no representation of dendritic processing. A recent study of standing and traveling waves in the Nunez model posed on a sphere can be found in [11]. Interestingly the Nunez model has a representation of space-dependent delays arising from the finite speed of action potential propagation along axons, and for certain patterns of decaying strength of non-local connectivity it can be formulated as a damped inhomogeneous wave equation [12]. This *brain-wave* equation, and variants thereof, has played a major role in the interpretation of EEG signals since the 1970s [13–17]. Moreover, the local nature of such models means that they are amenable to analysis with standard numerical techniques for partial differential equations (PDEs), circumventing the challenges of evolving delayed integro-differential models [12, 18].

With the advent of laminar electrodes to record from different layers of cortex [19] it is now timely to build on the original work of Bressloff, reviewed in [20], and develop neural field models that incorporate a notion of dendritic depth. Moreover, given the benefits of the brain-wave equation it is sensible to look for generalizations that can incorporate both axons and dendrites, as well as the patterns of connectivity between them. This is the topic that we address in this paper. We show how to develop the cable modeling approach of Rall [21] to describe a firing rate cortical tissue model with axo-dendritic patterns of synaptic connectivity, allowing for a

* james.ross1@nottingham.ac.uk
† m_margetts@btinternet.com
‡ i.bojak@reading.ac.uk
§ rachel.nicks@nottingham.ac.uk
¶ d.avitabile@vu.nl
** stephen.coombes@nottingham.ac.uk

mixture of excitatory and inhibitory synapses across the model of the dendritic tree. In doing so we obtain a natural extension of two-dimensional neural field models to include a third dimension representing position along a dendritic cable. The firing rate in the somatic (cell body) layer is taken to be a smooth sigmoidal function of the cable voltage at the soma, which is in turn determined by the spatio-temporal pattern of synaptic currents on the cable.

In §II we describe the formulation of the model in terms of a generalized neural field, prescribed by a given pattern of axo-dendritic connectivity. This tissue model is a continuum description of cell bodies arranged in a surface with each point *fibrated* by a simple one-dimensional model of a dendritic tree. The dynamics of the cell bodies is described with a delayed integro-differential equation. In turn this is used to drive activity in the dendrite along connected structural axonal pathways. The dynamics of the dendritic tree is considered to be *passive* and is modeled using the PDE approach of cable theory. Next, in §III, we exploit the fact that the strength of connections in large scale cortical structures is known to fall off exponentially with distance to reformulate the model as a set of coupled PDEs. These generalize the traditional brain-wave equation to include a notion of dendritic depth. Numerical simulations of this local PDE formulation are presented in §IV, with our numerical scheme validated against an exact traveling front solution that can be constructed in the limit of a steep sigmoidal firing rate. These simulations are used to highlight the effect that known correlations between the distance of connection along the dendrite and separation between cell bodies can have on the speed and shape of traveling waves. Finally in §V we discuss natural extensions of the work in this paper.

II. THE MODEL

We take as our model dendrite the standard one dimensional unbranched uniform cable equation, and distinguish between pyramidal cells and interneurons by introducing the labels P (for pyramidal) and I (for interneuron). The voltage $V_a(x,\mathbf{r},t)$ at position $x\in\mathbb{R}$ along an infinite passive cable of neuron type $a\in\{P,I\}$ with somatic coordinate $\mathbf{r}\in\mathbb{R}^2$ can then be written:

$$\frac{\partial V_a}{\partial t}=-\frac{V_a}{\tau_a}+D_a\frac{\partial^2 V_a}{\partial x^2}+I_a(x,\mathbf{r},t). \tag{1}$$

Here, τ_a is recognized as the membrane time-constant of the dendrite, and D_a as the cable diffusion coefficient. The *electrotonic length* $\sqrt{D_a\tau_a}$ of a dendrite is typically in the range $0.1-1$mm. Here, $I_a(x,\mathbf{r},t)$ is the synaptic input, which we shall split into an excitatory and inhibitory part:

$$I_a=g_{aP}(V_+-V_a)+g_{aI}(V_--V_a), \tag{2}$$

where $V_+=V_+(x)$ and $V_-=V_-(x)$ are positive and negative synaptic reversal potentials respectively that can vary across the dendritic cable. The conductance changes g_{ab} evolve according to a slightly modified neural field prescription as [2, 22]

$$g_{ab}(x,\mathbf{r},t)=\int_{-\infty}^{t}\mathrm{d}s\eta_{ab}(t-s)\times \int_{\mathbb{R}^2}\mathrm{d}\mathbf{r}'W_{ab}(x,\mathbf{r},\mathbf{r}')f_b(h_b(\mathbf{r}',s-|\mathbf{r}-\mathbf{r}'|/v_{ab})). \tag{3}$$

Here $\eta_{ab}(t)$ is an α-function synaptic filter

$$\eta_{ab}(t)=\alpha_{ab}^2 t\mathrm{e}^{-\alpha_{ab}t}H(t), \tag{4}$$

where H is the Heaviside step function. The time-to-peak for the α-function $\eta_{ab}(t)$ is α_{ab}^{-1}, and the parameter α_{ab} can be used to control the *speed* of the synapse. A *fast* synapse would have a typical time-to-peak of around 1ms, whilst a *slow* synapse would have a time-scale of around 100ms. The function $W_{ab}(x,\mathbf{r},\mathbf{r}')$ describes the axo-dendritic connectivity pattern between populations a and b, whilst v_{ab} is the velocity of the action potential propagated from population b to a. This speed can range from around 0.5m/s in unmyelinated axons to 150m/s in myelinated axons (in the peripheral nervous system), and typical values for cortico-cortical axonal speeds in humans are distributed, and appear to peak in the $5-10$ m/s range [23] though speeds in callosal fibres can range from $7-19$ m/s [18]. The field h_a is taken as a measure of the somatic activity in population a, whilst f_a describes the firing rate of population a. This latter function is often chosen to have a simple sigmoidal form, and we shall work with the choice $f_a(h)=[1+\exp(-\beta_a(h-\theta_a))]^{-1}$, where $\beta_a>0$ controls the steepness of f_a, and θ_a is a *threshold*. As a model of h_a we shall take the somatic potential, namely the voltage on the cable at the point where the cell body lies. We fix this to be the coordinate where $x=0$ so that $h_a(\mathbf{r},t)=V_a(0,\mathbf{r},t)$. A schematic of the neural field model incorporating dendrites is shown in Fig. 1 .

Assuming vanishing initial data, we may write the solution to (1) in the form

$$V_a(x,\mathbf{r},t)=(G_a\otimes I_a)(x,\mathbf{r},t), \tag{5}$$

where $G_a(x,t)$ is the Green's function

$$G_a(x,t)=\frac{1}{\sqrt{4\pi D_a t}}\mathrm{e}^{-x^2/(4D_a t)}\mathrm{e}^{-t/\tau_a}H(t), \tag{6}$$

and the operator $\otimes$ denotes spatio-temporal convolution over the (x,t) coordinates. Unfortunately equation (5) does not provide an explicit formula for V_a (and hence h_a) since I_a itself depends on V_a. However, by repeated substitution and truncating terms at second order in the conductances we have that

$$h_a(\mathbf{r},t)=(G_a\otimes[g_{aP}V_++g_{aI}V_-])(0,\mathbf{r},t) -(G_a\otimes\{[g_{aP}+g_{aI}]G_a\otimes[g_{aP}V_++g_{aI}V_-]\})(0,\mathbf{r},t), \tag{7}$$

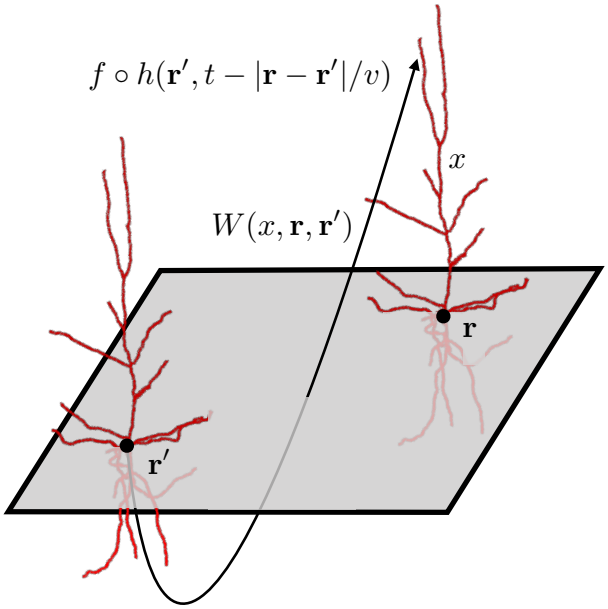

FIG. 1: A schematic of the neural field model incorporating dendrites. Here the dendrites are shown with realistic structure, though for simplicity we only consider idealized unbranched dendrites in the model formulation. The black filled circles indicate the position of the cell body or *soma*.

which shows that the dendrite acts to mix conductance changes (if input currents are shunted). The formula for h_a in equation (7) is in fact the first two terms in a Neumann series expansion and see [20] for a further discussion of this in the context of dendritic modeling.

To model cortical anatomy in a biologically plausible fashion we choose the distribution $W_{ab}(x, \mathbf{r}, \mathbf{r}') = W_{ab}(x, |\mathbf{r} - \mathbf{r}'|)$ with

$$W_{ab}(x, r) = W^0_{ab} w_{ab}(r) \delta(x - d_{ab} - \kappa_{ab} r), \tag{8}$$

where $r = |\mathbf{r}|$, $d_{ab}, \kappa_{ab} \in \mathbb{R}$ and $W^0_{ab} > 0$, which incorporates the fact that synapses are located further away from the soma as the separation between neurons increases [24]. For $\kappa_{ab} = 0$ there is no correlation between somatic and dendritic coordinates and synapses occur at a fixed distance d_{ab} from the soma. To complete the description of the neural tissue model we need only specify the form of the anatomical connectivity function $w_{ab}(r)$ that describes how the strength of the interactions changes with separation between cell bodies. Most long-range synaptic interactions are excitatory, with excitatory pyramidal cells sending their myelinated axons to other parts of the cortex. Inhibitory interactions, on the other hand, tend to be much more short-ranged. For excitatory connections between cortical areas in macaque monkeys the weight of connection between two areas decays approximately exponentially with their wiring distance, with a characteristic distance of $\sim$ 11mm [25], and for a nice overview of brain structure and dynamics across scales we recommend the article by Wang and Kennedy [26]. Hence, it is natural to choose an exponential form:

$$w_{ab}(r) = \frac{1}{2\pi\sigma^2_{ab}} \exp(-r/\sigma_{ab}), \tag{9}$$

with $\sigma_{aP} > \sigma_{aI}$ to respect the fact that in neocortex the extent of excitatory connections w_{aP} is broader than that of inhibitory connections w_{aI}.

III. GENERALIZED BRAIN-WAVE EQUATION

To numerically analyze the nonlinear integro-differential equation model with space-dependent delays given in §II, it is convenient to consider the development of a PDE model where evolution is expressed in terms of differential, rather than integral, operators. This is a common approach in analyzing neural field models that lack dendrites [27] because such models are numerically easier to simulate than non-local integral equations. This re-formulation in terms of a PDE essentially relies on the specific choice of the kernel (9) having certain properties, and the main one being that its Fourier transform can be well approximated by a rational function.

We make use of the fact that an α-function is the Green's function of a linear differential operator to write $Q_{ab}\eta_{ab} = \delta(t)$, where $Q_{ab} = (1 + \alpha^{-1}_{ab}\partial/\partial_t)^2$. Hence from (3) we obtain a PDE for g_{ab} as

$$Q_{ab} g_{ab} = \psi_{ab}, \tag{10}$$

with $g_{ab}(x, \mathbf{r}, 0) = 0$, $\partial g_{ab}/\partial t|_{t=0} = 0$ and

$$\psi_{ab}(x, \mathbf{r}, t) = \int_{-\infty}^{\infty} \mathrm{d}s \int_{\mathbb{R}^2} \mathrm{d}\mathbf{r}' \Omega_{ab}(x, |\mathbf{r} - \mathbf{r}'|, t - s) \times f_b(h_b(\mathbf{r}', s)), \tag{11}$$

where $\Omega_{ab}(x, r, t) = W_{ab}(x, r)\delta(t - r/v_{ab})$. Introducing a Fourier transform over the dendritic spatial coordinate allows us to represent a function $\phi(x, \mathbf{r}, t)$ in the form

$$\phi(x, \mathbf{r}, t) = \int_{-\infty}^{\infty} \frac{\mathrm{d}p}{2\pi} \mathrm{e}^{ipx} \widehat{\phi}(p, \mathbf{r}, t). \tag{12}$$

Using (8) we find that

$$\widehat{\psi}_{ab}(p, \mathbf{r}, t) = \int_{-\infty}^{\infty} \mathrm{d}s \int_{\mathbb{R}^2} \mathrm{d}\mathbf{r}' H_{ab}(p, |\mathbf{r} - \mathbf{r}'|, t - s) \times f_b \circ h_b(\mathbf{r}', s), \tag{13}$$

with

$$H_{ab}(p, r, t) = W^0_{ab} \mathrm{e}^{-ip[d_{ab} + \kappa_{ab} r]} w_{ab}(r) \delta(t - r/v_{ab}). \tag{14}$$

Taking further Fourier transforms with respect to $(\mathbf{r}, t)$ and introducing spectral parameters $(\mathbf{k}, \omega)$ we exploit the convolution structure of (13) to obtain

$$\widehat{\psi}_{ab}(p, k, \omega) = \widehat{H}_{ab}(p, k, \omega) \widehat{\rho}_b(k, \omega), \tag{15}$$

where $\rho_b = f_b \circ h_b$ and the Fourier transform of H_{ab} may be evaluated as

$$\widehat{H}_{ab}(p,k,\omega) = \frac{W^0_{ab}}{\sigma^2_{ab}} \frac{A_{ab}(p,\omega)}{(A^2_{ab}(p,\omega)+k^2)^{3/2}} \mathrm{e}^{-ipd_{ab}}, \quad (16)$$

and $A_{ab}(p,\omega) = 1/\sigma_{ab} + i\omega/v_{ab} + ip\kappa_{ab}$. After cross multiplying and using the long-wavelength approximation (namely expanding $\widehat{H}_{ab}(p,k,\omega)$ around $k=0$) and taking the inverse Fourier transform we obtain a PDE in 3 spatial dimensions (two for the somatic sheet and one for the dendritic cable):

$$\left[\mathcal{A}^2_{ab} - \frac{3}{2}\nabla^2\right]\psi_{ab}(x,\mathbf{r},t) = \frac{W^0_{ab}}{\sigma^2_{ab}} \times \delta(x-d_{ab}) f_b \circ h_b(\mathbf{r},t), \quad (17)$$

where

$$\mathcal{A}_{ab} = \frac{1}{\sigma_{ab}} + \frac{1}{v_{ab}}\frac{\partial}{\partial t} + \kappa_{ab}\frac{\partial}{\partial x}. \quad (18)$$

We interpret (17), coupled to (10) and (7), as the natural generalization of previous brain-wave equations of Nunez type, such as those in [28–30], to include dendritic processing. To work without the small conductance assumption one should use the PDE (1), instead of (7), with $h_a(\mathbf{r},t) = V_a(0,\mathbf{r},t)$. A similar analysis can be carried out for a model with a one-dimensional somatic space. Using z as the coordinate in the somatic space and choosing an anatomical connectivity function $w_{ab}(z) = \exp(-|z|/\sigma_{ab})/(2\sigma_{ab})$ we obtain, following the same approach as above, the PDE in 2 spatial dimensions (one for the somatic space and one for the dendritic cable):

$$\left[\mathcal{A}^2_{ab} - \frac{\partial^2}{\partial z^2}\right]\psi_{ab}(x,z,t) = \frac{W^0_{ab}}{\sigma_{ab}} \times \left[\left(\frac{1}{\sigma_{ab}} + \kappa_{ab}\frac{\partial}{\partial x} + \frac{1}{v_{ab}}\frac{\partial}{\partial t}\right)\delta(x-d_{ab})\right] f_b \circ h_b(z,t). \quad (19)$$

Unlike its higher dimensional counterpart this equation is *exact* since the long-wavelength approximation is not needed.

IV. NUMERICAL SIMULATIONS

To numerically evolve the new type of brain-wave equation described in §III it is natural to consider a finite-difference scheme to approximate spatial derivatives using central difference operations for second order derivatives, backward difference operations for first order derivatives and time-stepping that can be performed using an adaptive solver. For the latter we use a routine from the Julia package – DifferentialEquations.jl [31, 32]. The spatial domain is discretized into uniform rectangles with size $\Delta x \times \Delta z$ for the 2 dimensional model and cuboids with size $\Delta x \times \Delta r_1 \times \Delta r_2$ for the 3 dimensional model. The Fourier transforms in the derivation of the brain-wave equation rely on infinite spatial domains and therefore we need to consider carefully the boundary conditions employed in a practical setting. It is natural to consider a periodic somatic domain with a large period, using a ring for the model with a one-dimensional somatic space and a torus when the somatic space is two-dimensional. The cable equation may be imposed on a large finite domain with $x \in [X_-, X_+]$, and it is natural to choose closed end boundary conditions (so that the current is zero), that can be implemented as Neumann boundaries at $x = X_\pm$. The Dirac-delta function in (19) can be approximated with a thin narrow Gaussian $\delta_\varepsilon(x) = \exp(-x^2/\varepsilon^2)/\sqrt{\pi\varepsilon^2}$ with a fixed value of ε as the small dendritic spatial discretization size Δx. Further discussion of the numerical method is provided in Appendix A.

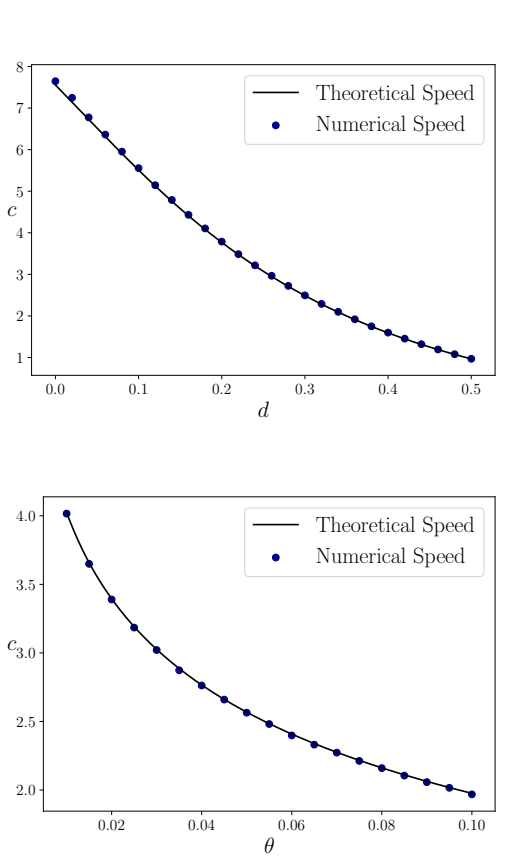

FIG. 2: Front wave speed (m/s) comparison of theory vs. numerical simulation for the model in 2 spatial dimensions (one somatic and one dendritic) with a Heaviside firing rate. Here the dendritic input current is $I(x,z,t) = g(x,z,t)$ and $\kappa = 0$ when (a) the input position d changes, and (b) the threshold of the Heaviside function θ changes. Parameters: $W^0 = 1$, $v = 8$ (m/s), $\alpha = 1$, $\Delta x = 0.01$, with $X_\pm = \pm 1$, (a) $\theta = 0.001$, and (b) $d = 0$.

To validate our numerical approach it is useful to consider a restriction of the model that allows for an exact solution, so that theory and numerics can be easily compared. One such reduction is to focus on the model in 2 dimensions given by (19), and treat only a single excitatory population with a Heaviside firing rate and with a large spatially uniform synaptic reversal potential. This latter restriction means that inputs are no longer state dependent, and, after absorbing a factor of V_+ within g_{PP}, that we may write $I_P = g_{PP}$. In this case, and fixing $\kappa_{PP} = 0$, it is possible to construct a traveling front solution whose speed c_{PP} is given by the implicit solution of

$$\theta_P = \frac{1}{2}\widetilde{G}\left(d_{PP}, \lambda\right)\widetilde{\eta}\left(\lambda\right), \quad \lambda = \frac{c_{PP} v_{PP}}{\sigma_{PP}\left(v_{PP} - c_{PP}\right)}. \quad (20)$$

Here θ_P is the threshold in firing rate function $f_P(h) = H(h - \theta_P)$, σ_{PP} is the spatial length scale for the exponential decay of connection strength, v_{PP} is the speed of the action potential, and d_{PP} is the contact distance of the synapse on the dendrite (as measured from the soma). The functions $\widetilde{G}(\cdot, \lambda)$ and $\widetilde{\eta}(\lambda)$ are the Laplace transforms $t \mapsto \lambda$ of G_P and η_{PP} given respectively by (6) and (4). These can be calculated explicitly as

$$\widetilde{G}(d_{PP}, \lambda) = \frac{\mathrm{e}^{-\gamma(\lambda) d_{PP}}}{2 D_P \gamma(\lambda)}, \qquad \gamma^2(\lambda) = \frac{1/\tau_P + \lambda}{D_P}, \quad (21)$$

$$\widetilde{\eta}(\lambda) = \frac{\alpha_{PP}^2}{(\alpha_{PP} + \lambda)^2}. \quad (22)$$

The derivation of (20) is given in Appendix B.

For the following numerical simulations we remove physical units by measuring space in units of σ_{PP} (the spatial scale for anatomical connectivity) and time in units of τ_P (the membrane time-constant of the cable). Thus we replace $D_P = D \cdot \sigma_{PP}^2/\tau_P$, $\alpha_{PP} = \alpha/\tau_P$, $d_{PP} = d \cdot \sigma_{PP}$ and $v_{PP} = v \cdot \sigma_{PP}/\tau_P$ in our equations and re-scale $x \to x \cdot \sigma_{PP}$, $r \to r \cdot \sigma_{PP}$ and $t \to t \cdot \tau_P$. This means also derived variables like Δx are to be considered as re-scaled in the following, e.g., $\Delta x = 0.1$ means $0.1 \cdot \sigma_{PP}$. For concreteness we shall consider $\sigma_{PP} = 10$mm and $\tau_P = 10$ms. Conveniently, in this case $\sigma_{PP}/\tau_P = 1$m/s and thus front wave speed $c_{PP} = c \cdot \sigma_{PP}/\tau_P$ has the same numeric value in units of m/s as the unit-free c. In figure captions we will show the physical units in brackets "(m/s)" as equivalent for our specific choice. Unless otherwise stated, we shall also fix the electrotonic distance $\sqrt{D_P \tau_P} = \sqrt{D}\sigma_{PP}$ to be $0.1\sigma_{PP} = 1$mm, i.e., $D = 0.01$.

In Fig. 2 we show a plot of the theoretical wave front speed, using (20), against direct numerical simulations obtained using the numerical scheme described above. The periodic somatic spatial domain is chosen sufficiently large to allow for the full formation of fronts, whilst the size of the dendritic domain is chosen in relation to its electrotonic length such that $|d - X_\pm| > \sqrt{D}$. There is excellent agreement between theory and simulations under parameter variation in both d (the dendritic contact distance of the synapse from the soma) and θ (the threshold in the Heaviside firing rate function). We take this as validation of the proposed finite difference scheme, and re-use the same numerical methodology to explore the behaviour of the model in more general settings, with a sigmoidal firing rate, finite synaptic reversal potential, and non-zero correlation parameter κ.

In Fig. 3 we further consider the 2 dimensional model (with a one-dimensional somatic space) using a sigmoidal firing rate. Here we observe travelling waves in both the conductance and voltage. Activity clearly spreads along the somatic space and decays in the dendritic space (as expected from the diffusive nature of the cable equation). The effect of increasing κ on the speed of the front for

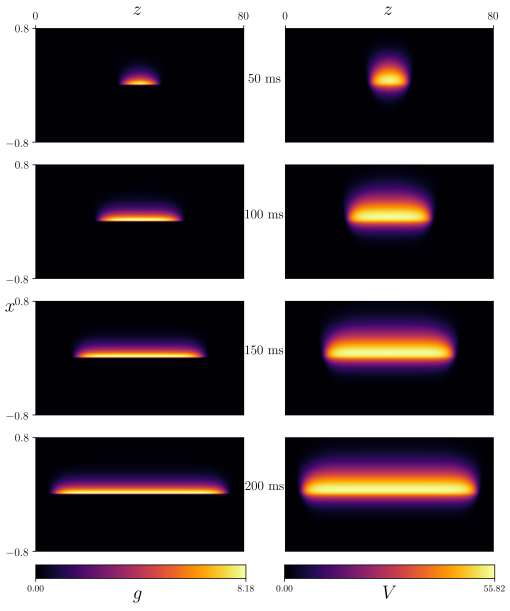

FIG. 3: Travelling wave in the model with 2 spatial dimensions (one somatic and one dendritic) shown for conductance (left) and voltage (right) with a shunted current $I(x, z, t) = (V_+ - V(x, z, t))g(x, z, t)$ and a sigmoidal firing rate. Parameters: $V_+ = 70$mV, $W^0 = 1$, $\kappa = 0.1$, $v = 8$ (m/s), $\alpha = 1$, $\Delta x = 0.01$, $d = 0.02$, $X_\pm = \pm 0.8$, $\beta = 100$, and $\theta = 0.15$.

a Heaviside firing rate is quantified in Fig. 4. The results from these numerical experiments show that the wave speed decreases with increasing κ (for all values of d). In Fig. 5 the effects of changing the time-to-peak of the synapse α^{-1} is shown. Here we see that the wave front speed decreases as the synapse becomes slower. In Fig. 6 we show that an increase in the excitatory synaptic reversal potential causes an increase in wave front speed. When considering the variation of the correlation strength κ we find that for $\kappa = 0$ the peak of the wave response along the dendrite occurs at a distance d from the soma, as expected. However, with an increase

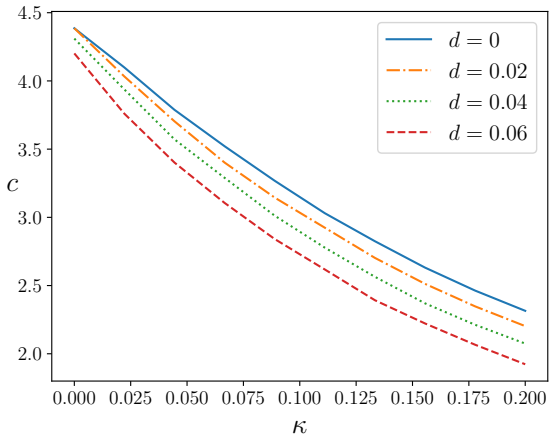

FIG. 4: Wave front speed (m/s) as the correlation strength κ is increased for various values of the synaptic contact parameter d with $I(x, z, t) = g(x, z, t)$ and a Heaviside firing rate function. Parameters: $W^0 = 5$, $v = 8$ (m/s), $\alpha = 1$, $\Delta x = 0.02$, $X_\pm = \pm 1$, and $\theta = 0.01$.

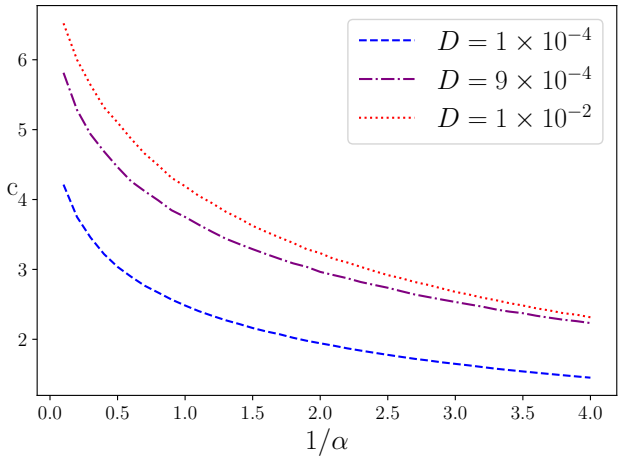

FIG. 5: Wave front speed (m/s) with an increase in the synaptic time-to-peak α^{-1} with $I(x, z, t) = g(x, z, t)$, a Heaviside firing rate, and three differing electrotonic lengths. Parameters: $W^0 = 3$, $\kappa = 0$, $v = 8$ (m/s), $\Delta x = 0.01$, $d = 0.03$, $X_\pm = \pm 0.5$, and $\theta = 0.01$.

in κ this peak response shifts slightly away from d to a larger distance from the soma. We illustrate this effect in Fig. 7, where we also see an increase in the width of the activity that spreads into the dendrite away from the contact point at $x = d$. Finally, in Fig. 8 we consider the 3 dimensional model (with a two-dimensional somatic space) using a sigmoidal firing rate. Here we show a traveling wave propagating from the centre of the domain. Similarly as for the 2 dimensional model, see Fig. 3, the activity clearly spreads through the somatic layer, and decays along the dendrite at large distances from the cell body.

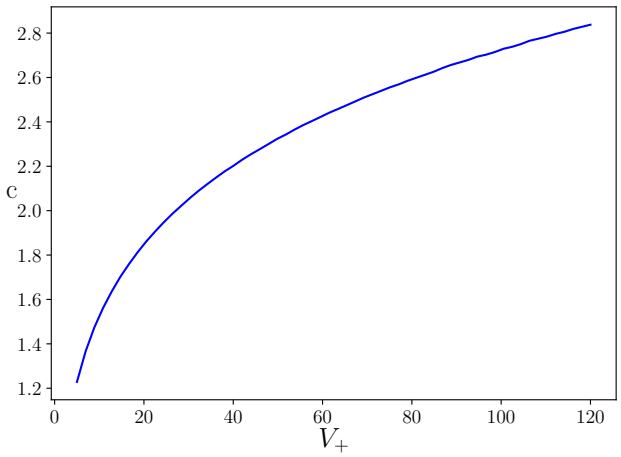

FIG. 6: Wave front speed (m/s) in a model with a shunted current $I(x, z, t) = (V_+ - V(x, z, t))g(x, z, t)$ as a function of the excitatory synaptic reversal potential V_+ (mV), with a sigmoidal firing rate. Parameters: $W^0 = 4$, $\kappa = 0.1$, $v = 8$ (m/s), $\alpha = 1$, $\Delta x = 0.01$, $d = 0.04$, $X_\pm = \pm 0.5$, $\beta = 100$, and $\theta = 0.15$.

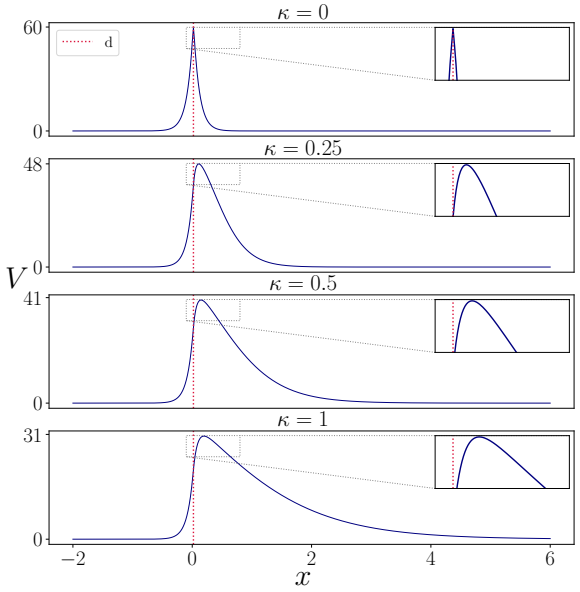

FIG. 7: Slices along the x dimension of a voltage front where it can be seen that increasing κ causes the peak response to shift away from d (marked as the red vertical dotted line) and away from the soma. Parameters: $V_+ = 70$mV, $W^0 = 4$, $v = 8$ (m/s), $\alpha = 1$, $\Delta x = 0.01$, $d = 0.02$, $X_- = -2$, $X_+ = 6$, $\beta = 100$, and $\theta = 0.1$.

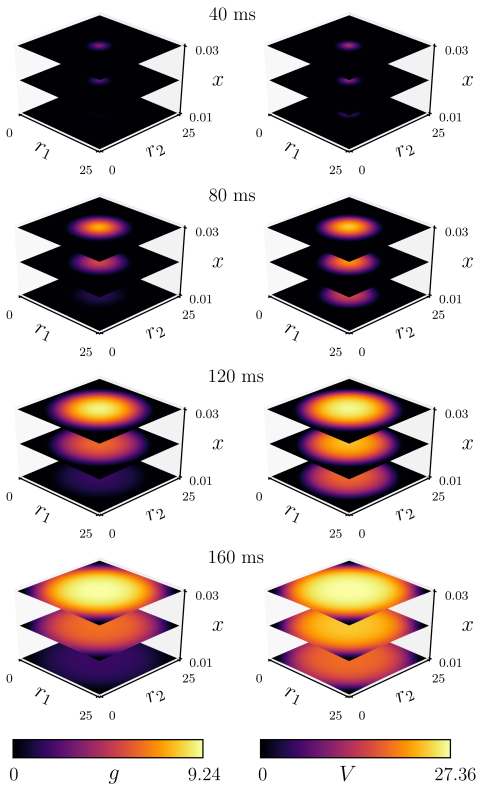

FIG. 8: Travelling wave in the 3 dimensional model (two somatic and one dendritic), with a sigmoidal firing rate, shown for conductance (left) and voltage (right) with $I(x,z,t) = (V_+ - V(x,z,t))g(x,z,t)$. Parameters: $V_+ = 70$mV, $W^0 = 1$, $\kappa = 0.1$, $v = 8$ (m/s), $\alpha = 1$, $\Delta x = 0.01$, $d = 0.02$, $X_\pm = \pm 0.5$, $\beta = 100$, and $\theta = 0.15$.

V. DISCUSSION

In this paper we have introduced a generalization of the Nunez brain-wave equation to account for passive dendritic processing. This is potentially important for the understanding of real EEG data given that this is known to arise from the addition of dipole moments generated by sinks and sources on dendrites. The generalised model bridges multiple scales, combining local models of dendrites with global models of synaptic and firing rate activity with both distributed (synaptic) and space-dependent (axonal) delays, emphasising that dendritic response (Green's) functions can lead to another form of distributed delay that shapes emerging spatio-temporal network patterns. As well as being relevant to EEG the finer detail of the local model (with a spatially extended dendrite) makes it relevant to recorded potentials arising in electrocorticography (ECoG) and local field potential (LFP) recordings, with spatial resolution of $2-5$mm for ECoG and $0.1-1$mm for LFP, contrasting with the $20-30$mm of (high resolution) EEG.

We have shown that the model is readily simulated using standard finite difference schemes for PDEs, and validated one proposed scheme against an exact traveling front solution. We have performed parameter studies for the effects of system parameters on the speed of traveling fronts, and shown that correlations between somatic and dendritic coordinates in axo-dendritic connectivity patterns can strongly affect the speed of a wave. With an increase in the correlation parameter κ we see a slow down in the speed of the wave and the peak response shifts further away from the soma.

For deployment in a neuroscience setting it is interesting to consider further work to optimize parameters of the model to fit real data. In this regard it is natural to extend previous work of Bojak and Liley, using Particle Swarm Optimization, to generate EEG power spectra densities (PSDs) similar in shape to the ones observed in humans [33]. Such PSDs can be generated analytically using a noise-driven linear response theory as well as numerically thorough simulation of the full PDE model, after the inclusion of a noise source in equation (2). Importantly this would shed light on how real patterns of axo-dendritic connectivity can shape PSDs, as well as the known scaling of synaptic strength with distance from the soma that underlies so-called *dendritic democracy* [34]. Moreover, the model can also be used to generate a more direct measure of EEG, by recognising that the currents along the dendrites can be used to construct electromagnetic fields [9, 35]. The transmembrane current $I_a^{\rm mem}$ at a point on the cable is equal to $1/r_a \partial^2 V_a/\partial x^2$, where r_a is the (constant) specific resistance per unit length for currents flowing along the dendrite (and $r_a = 4R_a/(\pi d^2)$, where d is the diameter of the dendrite and R_a its axial resistivity). If the extracellular medium is assumed to be homogeneous, purely resistive and infinite in extent with conductivity σ_e, then the potential Φ arising from the transmembrane currents is (in the quasi-steady approximation to Maxwell's equations) given by

$$\Phi(x,\mathbf{r},t) = \frac{1}{4\pi\sigma_e}\sum_a \int_{-\infty}^{\infty} \mathrm{d}x' \int_{\mathbb{R}^2} \mathrm{d}\mathbf{r}' \frac{I_a^{\rm mem}(x',\mathbf{r}',t)}{d(x,x',\mathbf{r},\mathbf{r}')}, \tag{23}$$

where $d(x,x',\mathbf{r},\mathbf{r}') = \sqrt{(x-x')^2 + |\mathbf{r}-\mathbf{r}'|^2}$ is a simple notion of distance. Indeed Φ might give a more apt description of the fields observed using laminar implanted electrodes [36]. One final generalization of the work in this paper would be to treat more realistic models of dendrites. From a morphological perspective this could be incorporated by replacing the Green's function of the simple cable by one for a branched system. This can be constructed analytically using the *sum-over-trips* formalism, that itself can also cope with *quasi-active* membrane models (describing the resonance properties of dendrites associated with certain nonlinear ionic currents) [37]. All of the above are topics of ongoing research and will be

reported upon elsewhere.

Appendix A: Numerical Method

Here we describe the numerical scheme for evolving a single population with only excitatory interactions. This allows us to suppress the indices a, b, although the extension to include inhibition is straightforward by generalising the scheme below (and using the index notation of §II). We note that expanding the differential operator $\mathcal{A}^2$ in equations (17) and (19) gives rise to a 'negative diffusion' term, that, if not handled sensibly, could give rise to numerical instabilities. To circumvent this potential issue we write $\mathcal{A}^2\psi$ in the coupled form $\mathcal{A}^2\psi = \mathcal{A}y$, where $y = \mathcal{A}\psi$. After discretizing in space the model in 2 spatial dimensions given by (19) takes the form of a system of coupled first order ordinary differential equations that we can write as

$$\frac{\mathrm{d}Y_1}{\mathrm{d}t} = -v\left(\frac{1}{\sigma}U + k\Delta_x^{(b)}U - \Delta_{zz}^{(c)}\psi \right. \tag{A1}$$
$$\left. -\frac{W^0}{\sigma^2}f(V_0-h)\delta(x-d) - \frac{W^0\kappa}{\sigma}\Delta_x^{(b)}f(V_0-h)\delta(x-d)\right),$$

$$\frac{\mathrm{d}\psi}{\mathrm{d}t} = -v\left(\frac{1}{\sigma}\psi + k\Delta_x^{(b)}\psi - U\right), \tag{A2}$$

$$\frac{\mathrm{d}Y_2}{\mathrm{d}t} = \alpha(\psi - Y_2), \tag{A3}$$

$$\frac{\mathrm{d}g}{\mathrm{d}t} = \alpha(Y_2 - g), \tag{A4}$$

$$\frac{\mathrm{d}V}{\mathrm{d}t} = -\frac{V}{\tau} + D\Delta_{xx}^{(c)}V + I, \tag{A5}$$

where $I = g(V_+ - V)$, $U = Y_1 + W^0 f(V_0 - h)\delta(x - d)/\sigma$, $V_0 = V(0, z, t)$, and $\Delta_x^{(b)}$ is the first order backwards difference operator acting on x, and $\Delta_{xx}^{(c)}$ and $\Delta_{zz}^{(c)}$ are the second order central difference operators in the x and z directions respectively. Here the variables (Y_1, ψ, Y_2, g, V) are interpreted as vectors on the corresponding (uniform) spatial meshes.

A similar approach may be taken for the 3 dimensional model given by (17) and yields essentially the same equations with finite-difference operators along the z direction replaced by the Kronecker sum of the second order central difference operators along the r_1 and r_2 directions which we denote by $\Delta_{\mathbf{rr}}^{(c)}$, and the further replacement:

$$\frac{\mathrm{d}Y_1}{\mathrm{d}t} = -v\left(\frac{1}{\sigma}Y_1 + k\Delta_x^{(b)}Y_1 - \frac{3}{2}\Delta_{\mathbf{rr}}^{(c)}\psi - \right. \tag{A6}$$
$$\left. \frac{W}{\sigma^2}f(V_0-h)\delta(x-d)\right),$$

$$\frac{\mathrm{d}\psi}{\mathrm{d}t} = -v\left(\frac{1}{\sigma}\psi + k\Delta_x^{(b)}\psi - Y_1\right). \tag{A7}$$

Here $V_0 = V(0, \mathbf{r}, t)$. The time integration was performed using an adaptive solver from the Julia package – DifferentialEquations.jl [31, 32].

Appendix B: Front speed in the Heaviside limit

Here we consider an idealized dendritic neural field model in a one dimensional cortex model with a Heaviside firing rate and only excitatory interactions. In the absence of any shunts (namely setting the input to the cable to be directly proportional to the conductance change) this allows an exact calculation of the speed of a front. The cable voltage evolves according to (1) with input $I = I_P$:

$$\left(1 + \frac{1}{\alpha}\frac{\partial}{\partial t}\right)^2 I(x,z,t) = \int_{-\infty}^{\infty}\mathrm{d}z' w(z-z')\times$$
$$\delta(x - d - \kappa|z-z'|)f\circ h(z', t-|z-z'|/v), \tag{B1}$$

where $h(z,t) = V(0,z,t)$, we have fixed $W^0 = 1$ and $f(h) = H(h-\theta)$. Above and throughout this Appendix we drop all subscripts P and PP for ease of notation. However, the quantities in this Appendix are not to be confused with the unit-free notation introduced in §IV, and for clarity the subscripts are used there, cf. equations (20) to (22). Using the Green's function (6) the solution for $V(x,z,t)$ is given by (dropping initial data)

$$V(x,z,t) = \int_{-\infty}^{\infty}\mathrm{d}y\int_{-\infty}^{t}\mathrm{d}s G(x-y,t-s)I(y,z,s). \tag{B2}$$

Hence, combining the above, we may write the evolution equation for the somatic potential $h(z,t)$ in the integral form

$$h(z,t) = \int_{-\infty}^{\infty}\mathrm{d}y\int_{-\infty}^{\infty}\mathrm{d}z'\int_0^{\infty}\mathrm{d}s\int_0^{\infty}\mathrm{d}s'\times$$
$$G(y,s)w(z')\delta(y-d-\kappa|z'|)\eta(s')\times$$
$$f\circ h(z-z', t-s-s'-|z'|/v), \tag{B3}$$

where $\eta(t) = \alpha^2 t\mathrm{e}^{-\alpha t}H(t)$. We now look for traveling wave solutions of the form $h(z,t) = h(\xi)$, where $\xi = z - ct$. These satisfy the integral equation

$$h(\xi) = \int_0^{\infty}\mathrm{d}s\eta(s)\psi_1(\xi + cs), \tag{B4}$$

where

$$\psi_1(\xi) = \int_{-\infty}^{\infty}\mathrm{d}z\int_0^{\infty}\mathrm{d}s G(d+\kappa|z|, s)w(|z|)\times$$
$$f\circ h(\xi - z + cs + c|z|/v). \tag{B5}$$

For the choice $\kappa = 0$ the double integral in (B5) simplifies to give

$$\psi_1(\xi) = \int_0^{\infty}\mathrm{d}s G(d,s)\psi_2(\xi + cs), \tag{B6}$$

where

$$\psi_2(\xi) = \int_{-\infty}^{\infty}\mathrm{d}z w(z)H[h(\xi - z + c|z|/v) - \theta]. \tag{B7}$$

We now consider traveling front solutions with $h(\xi) > \theta$ for $\xi < 0$ and $h(\xi) \leq \theta$ for $\xi \geq 0$. In this case we may evaluate (B7) as

$$\psi_2(\xi) = \begin{cases} \int_{\frac{\xi}{1-c/v}}^{\infty} \mathrm{d}z w(z) & \xi \geq 0 \\ \int_{\frac{\xi}{1+c/v}}^{\infty} \mathrm{d}z w(z) & \xi < 0 \end{cases}. \tag{B8}$$

The speed of the front is then determined self-consistently from the condition $h(0) = \theta$. This gives an implicit equation for the wave speed c as the solution to

$$\theta = \int_0^{\infty} \mathrm{d}s \eta(s) \psi_1(cs). \tag{B9}$$

To calculate the above we need only calculate $\psi_2(\xi)$ for $\xi \geq 0$. For an exponentially decaying anatomical connectivity function $w(z) = \exp(-|z|/\sigma)/(2\sigma)$ we have that

$$\psi_2(\xi) = \frac{1}{2} \exp\left(-\frac{\xi}{\sigma(1-c/v)}\right), \qquad \xi \geq 0. \tag{B10}$$

After introducing the Laplace transform $\widetilde{G}(d,\lambda) = \int_0^{\infty} \mathrm{d}s G(d,s) \mathrm{e}^{-\lambda s}$ this means that we may construct $\psi_1(\xi)$ from (B5) in the form

$$\psi_1(\xi) = \frac{1}{2} \widetilde{G}\left(d, \frac{c}{\sigma(1-c/v)}\right) \exp\left(-\frac{\xi}{\sigma(1-c/v)}\right). \tag{B11}$$

Substitution of (B11) into (B9) yields equation (20), where $\widetilde{\eta}(\lambda) = \int_0^{\infty} \mathrm{d}s \eta(s) \mathrm{e}^{-\lambda s}$ is the Laplace transform of $\eta(t)$.

[1] H. Berger, ArchPsych **87**, 527 (1929).
[2] S. Coombes, P. P. Beim Graben, R. Potthast, and J. Wright, *Neural fields : Theory and Applications* (Springer, 2014) p. 487.
[3] P. C. Bressloff, Journal of Physics A: Mathematical and Theoretical **45**, 033001 (2012).
[4] A. D. Steyn-Ross and M. Steyn-Ross, eds., *Modeling Phase Transitions in the Brain* (Springer, 2010).
[5] A. Hutt, M. Bestehorn, and T. Wennekers, Network **14**, 351 (2003).
[6] S. Coombes, N. A. Venkov, L. Shiau, I. Bojak, D. T. J. Liley, and C. R. Laing, Physical Review E **76**, 051901 (2007).
[7] I. Bojak, T. F. Oostendorp, A. T. Reid, and R. Kötter, Brain Topography **23**, 139 (2010).
[8] F. L. da Silva and A. Rotterdam, Electroencephalography: Basic principles, clinical applications and related fields (Lippincott Williams & Wilkins, 2005) Chap. Biophysical aspects of EEG and Magnetoencephalogram generation, pp. 107–126.
[9] K. H. Pettersen and G. T. Einevoll, Biophysical Journal **94**, 784 (2008).
[10] P. L. Nunez, Mathematical Biosciences **21**, 279 (1974).
[11] S. Visser, R. Nicks, O. Faugeras, and S. Coombes, Physica D **349**, 27 (2017).
[12] V. K. Jirsa and H. Haken, Physica D **99**, 503 (1997).
[13] P. L. Nunez, *Neocortical Dynamics and Human EEG Rhythms* (Oxford University Press, 1995).
[14] V. K. Jirsa, K. J. Jantzen, A. Fuchs, and J. A. S. Kelso, IEEE Transactions on Medical Imaging **21**, 493 (2002).
[15] P. L. Nunez and R. Srinivasan, *Electric Fields of the Brain: The Neurophysics of EEG*, 2nd ed. (Oxford University Press, New York, 2005).
[16] J. Daunizeau, S. J. Kiebel, and K. J. Friston, NeuroImage **47**, 590 (2009).
[17] R. G. Abeysuriya and P. A. Robinson, Journal of Neuroscience Methods **258**, 28 (2016).
[18] I. Bojak and D. T. J. Liley, PLoS Computational Biology **6**, e1000653 (2010).
[19] A. Maier, G. K. Adams, C. Aura, and D. A. Leopold, Frontiers in Systems Neuroscience **4** (2010).
[20] P. C. Bressloff and S. Coombes, International Journal of Modern Physics B **11**, 2343 (1997).
[21] I. Segev, J. Rinzel, and G. M. Shepherd, eds., *The theoretical foundations of dendritic function: selected papers of Wilfrid Rall with commentaries* (MIT Press, 1995).
[22] S. Coombes, G. J. Lord, and M. R. Owen, Physica D **178**, 219 (2003).
[23] P. L. Nunez and R. Srinivasan, Brain Research **1542**, 138 (2014).
[24] P. C. Bressloff, Physical Review Letters **76**, 4644 (1996).
[25] N. T. Markov, P. Misery, A. Falchier, C. Lamy, J. Vezoli, R. Quilodran, M. A. Gariel, P. Giroud, M. Ercsey-Ravasz, L. J. Pilaz, C. Huissoud, P. Barone, C. Dehay, Z. Toroczkai, D. C. Van Essen, H. Kennedy, and K. Knoblauch, Cerebral Cortex **21**, 1254 (2010).
[26] X.-J. Wang and H. Kennedy, Current Opinion in Neurobiology **37**, 92 (2016).
[27] S. Coombes, NeuroImage **52**, 731 (2010).
[28] P. A. Robinson, C. J. Rennie, and J. J. Wright, Physical Review E **56**, 826 (1997).
[29] M. L. Steyn-Ross, D. A. Steyn-Ross, J. W. Sleigh, and D. T. J. Liley, Physical Review E **60**, 7299 (1999).
[30] D. T. J. Liley, P. J. Cadusch, and M. P. Dafilis, Network **13**, 67 (2002).
[31] J. Bezanson, A. Edelman, S. Karpinski, and V. Shah, SIAM Review **59**, 65 (2017).
[32] C. Rackauckas and Q. Nie, Journal of Open Research Software **5**, 15 (2017).
[33] I. Bojak and D. T. J. Liley, Physical Review E **71**, 041902 (2005).
[34] M. Häusser, Current Biology **11**, R10 (2001).
[35] E. Hagen, S. Naess, T. V. Ness, and G. T. Einevoll, Frontiers in Neuroinformatics **12**, 92 (2018).
[36] A. M. Bastos, R. Loonis, S. Kornblith, M. Lundqvist, and E. K. Miller, Proceedings of the National Academy of Sciences **115**, 1117 (2018).
[37] S. Coombes, Y. Timofeeva, C.-M. Svensson, G. J. Lord, K. Josić, S. J. Cox, and C. M. Colbert, Biological Cybernetics **97**, 137 (2007).